Robust 3-D Wireless Power Transfer System Based on Rotating Fields for Multi-User Charging

Nelson Xuntuo Wang, *Student Member, IEEE*, Han-Wei Wang, *Student Member, IEEE*, Jie Mei, *Student Member, IEEE*, Sajjad Mohammadi, *Student Member, IEEE*, Jinyeong Moon, *Senior Member, IEEE*, Jeffrey H. Lang, *Fellow, IEEE*, and James L. Kirtley Jr., *Life Fellow, IEEE*

***Abstract*—A wireless power transfer system for multi-user charging is proposed to demonstrate a robust quasi-uniform power efficiency in a 3-D space. It employs a set of balanced magnetic coils excited with phase-shifted currents on the transmitting side to feature omnidirectionality. In this article, two transmitter structures, 2-coil and 3-coil systems are discussed and compared. These systems produce a quasi-uniform magnetic field magnitude regardless of the locations of the receiving coils provided that the coils point to the center of the transmitting system sphere at the same distance. A simulation platform is established for the proposed method. Experimental results at 2MHz substantiate a uniform spatial efficiency and bound the average error of analytical calculations within 10%. Furthermore, the proposed method with rotating fields based on phase-shifted currents shows that the 3-coil system yields a higher efficiency and a lower efficiency spread, 6.8% improvement on average efficiency and 88.7% reduction on efficiency variance, compared to the 2-coil system.**

***Index Terms*—Rotating field, wireless power transfer (WPT), resonant WPT, uniform magnetic field, robust efficiency, position-free, multi-user charging.**

I. Introduction

RESEARCHERS have put in considerable efforts to develop wireless power transfer (WPT) systems over the past decade. Following the first demonstration of efficient long-distance WPT in [1], achieved by making the inductive circuits resonate at the same frequency, subsequent papers [2]–[12] investigated the same approach, strengthening the resonant charging concept. Later, researchers developed multi-user charging [13]–[14] to meet the increasing need for charging more than one electronic devices at the same time. Due to their ubiquity, smart phones, for example, are increasingly in need of group charging in venues ranging from coffee shops to airports, however the locations of smart phones cannot be adjusted in such papers. The objective of this paper is to provide a quasi-uniform charging efficiency throughout all space around the transmitter, enabling multiple users to efficiently receive power regardless of device locations.

Resonant WPT, which has been applied to various applications, is fundamental to achieving high-efficiency power transfer between two sets of coils. For example, [6] focuses on the biomedical applications, [7] focuses on flying drone applications, [9]–[10] focus on electric motor applications, [15]–[16] introduce several methods to track and increase system efficiency, and [17]–[18] focus on network applications. The WPT system proposed here is distinct from those discussed above, it employs rotating magnetic fields to improve efficiency and is applicable to smart phones, tablets, multimedia devices, and even low-power laptops.

Magnetic MIMO [22]–[23] was developed for position-free charging applications. To enable charging of multiple users, adaptive algorithms based on user-detection are developed in [13], but the uniformity of power distribution is not considered. Thus, even though the overall efficiency is maximized, some users might be incapable of receiving power. Another method referred to as omnidirectional WPT eliminated blind spots in 2-D and 3-D spaces [24]. The single-user efficiency distribution using a phase-shifted current is studied in [25]. The current control to achieve optimized power efficiency is studied in [27]–[29]. The rotational and directional magnetic field of an omnidirectional WPT system is studied in [28]. However, the efficiency uniformity and power distribution among multiple users are not studied.

An advantage of the proposed system is a quasi-uniform efficiency in a 3-D space by employing rotating fields, produced like multi-phase electric machines [30]–[33]. Two different types are developed and studied: a 2-coil system with a phase shift of 90 degrees between the coil currents, and a 3-coil system with a phase shift of 120 degrees between the coil currents.

Manuscript received December 13, 2019; revised May 19, 2020 and September 15, 2020; accepted October 13, 2020. Date of publication October 29, 2020; date of current version May 21, 2021. This Manuscript is a Revised and enhanced version from an accepted Conference Award paper no. 0161 which won the best Demonstration Award at International Conference PowerMEMS (https://powermems2018.org) held in Florida USA in Dec. 2018. Paper no. TEC-01215-2019. *(Corresponding authors: Nelson Xuntuo Wang; Jie Mei.)*

Nelson Xuntuo Wang, Jie Mei, Sajjad Mohammadi, Jeffrey H. Lang, and James L. Kirtley Jr. are with the the Department of Electrical Engineering and Computer Science, Massachusetts Institute of Technology, Cambridge, MA 02139 USA (e-mail: nwang@mit.edu; jiemei@mit.edu; sajjadm@mit.edu; lang@mit.edu; kirtley@mit.edu).

Han-Wei Wang is with the Department of Electrical and Computer Engineering, University of Illinois at Urbana-Champion, IL USA (e-mail: hanweiw2@illinois.edu).

Jinyeong Moon is with the Department of Electrical and Computer Engineering, Florida State University, Tallahassee, FL 32310 USA (e-mail: j.moon@fsu.edu).

This article has supplementary downloadable material available at https://ieeexplore.ieee.org, provided by the authors.

Color versions of one or more of the figures in this article are available online at https://ieeexplore.ieee.org.

Digital Object Identifier 10.1109/TEC.2020.3034794

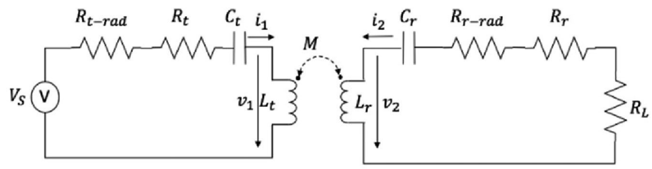

Fig. 1. Circuit model of an STSR system.

The phase-shifted currents create a uniform rotating magnetic field around the coils and provides a seamless power transfer to the multiple receivers in the charging space. This phase-shifting method creates the uniform efficiency in the space, which cannot be achieved by using a traditional non-phase shifting method. [34] introduced a 2-transmitter method, but it only works in 2-D and the quasi-uniform efficiency fluctuates beyond 10%, while the proposed methods in this paper present a uniform field in 2-D and a quasi-uniform field in 3-D, and an extremely low fluctuation in efficiency with up to 88.7% reduction on efficiency variance with a 3-transmitter structure.

The remainder of this paper is structured as follows. Section II outlines the theoretical underpinnings of the proposed WPT system. Analysis begins with an equivalent circuit diagram model, and then progresses to the development of relationships between key parameters derived for the convenience of understanding the system. This is followed by the modeling and analysis of the magnetic field distribution and charging efficiency for various use cases is discussed. A detailed benchmark comparison is presented to demonstrate the advantages of the proposed system over other methods. Section III presents the results of simulations and experiments. Two cases, one with a 2-coil transmitting structure and the other with a 3-coil transmitting structure, are examined and compared. Discrepancies between the theoretical expectations and the experimental results are examined. Section IV provides a summary and conclusions.

II. Modeling and Control

A. *Circuit Model*

1) Single-Transmitter Single-Receiver (STSR) System: Consider first the single-transmitter and single-receiver (STSR) case shown in Fig. 1. The magnetic coupling of the circuit can be described as below:

$$\begin{bmatrix} \mathrm{v}_1 \\ \mathrm{v}_2 \end{bmatrix} = \mathrm{j}\omega[\begin{matrix} \mathrm{L_t} & M \\ M & \mathrm{L_r} \end{matrix}]\begin{bmatrix} \mathrm{i}_1 \\ \mathrm{i}_2 \end{bmatrix}. \quad (1)$$

The secondary voltage is therefore:

$$\mathrm{v}_2 = -\left(\mathrm{R_r} + \mathrm{R_{r-rad}} + \mathrm{R_L} + \frac{1}{\mathrm{j}\omega \mathrm{C_r}}\right)\mathrm{i}_2 \quad (2)$$

where $\mathrm{R_r}$ is the resistance of the receiving coil, $\mathrm{R_L}$ is the load resistance, $\mathrm{C_r}$ is the resonant capacitance, and $\mathrm{R_{r-rad}}$ is the equivalent radiation resistance of the receiving coil. The radiation resistance, caused by the radiation of electromagnetic waves, is defined as the ratio of radiation power over current squared. Since the radius of the transmitting (Tx) coil (10 cm) is much smaller than the wavelength of radiation (150 m), $\mathrm{R_{r-rad}}$ can be approximated as a magnetic dipole. The radiation power of the magnetic dipole is $\frac{\mu_0\omega^4|\mathrm{m}|^2}{12\pi \mathrm{c}^3}$, where μ_0 is the permeability of free space, ω is the angular frequency, c is speed of light, and m is the magnetic dipole moment [3]. For the Tx coil, the magnetic dipole moment is proportional to its winding turns n, coverage area $\pi\alpha^2$, namely $\mathrm{n}\pi\alpha^2$. Thus $\mathrm{R_{r\text{-}rad}}$ can be further obtained as

$$\mathrm{R_{r-rad}} = \frac{\mathrm{P}}{|\mathrm{I}|^2} = \frac{\mu_0\omega^4|\mathrm{m}|^2}{12\pi\mathrm{c}^3} \Big/ |\mathrm{I}|^2 = \frac{\mathrm{n}^2\mu_0\omega^4\pi\alpha^4}{12\mathrm{c}^3}, \quad (3)$$

where α is radius of the coil, and n is the number of winding turns. When the frequency is on the order of MHz, α is on the order of 10 cm, and n is on the order of 10, $\mathrm{R_{r-rad}}$ becomes on the order of $10^{-7}\Omega$, and is thus negligible at MHz frequencies; however, $\mathrm{R_{r-rad}}$ is proportional to the 4$^{\text{th}}$ power of the frequency ω, thus if the frequency increases to 10 MHz, for example, the radiation resistance increases to a $\mathrm{m}\Omega$ level, and becomes comparable to the coil resistance.

At the resonance frequency of the transmitting and receiving coils, combining (1) and (2) yields

$$\frac{\mathrm{i}_1}{\mathrm{i}_2} = \frac{\mathrm{R_r} + \mathrm{R_{r-rad}} + \mathrm{R_L}}{\omega \mathrm{M}}, \quad (4)$$

which is the ratio of the transmitting coil current to the receiving coil current. The efficiency is defined as the ratio of the output power to the input power of the transmitting system, which is given by

$$\eta = \frac{\mathrm{i}_2 \times \mathrm{i}_2{}^* \cdot \mathrm{R_L}}{\mathrm{i}_1 \times \mathrm{i}_1{}^* \cdot (\mathrm{R_t} + \mathrm{R_{t-rad}}) + \mathrm{i}_2 \times \mathrm{i}_2{}^* \cdot (\mathrm{R_r} + \mathrm{R_{r-rad}} + \mathrm{R_L})}, \quad (5)$$

where $\mathrm{R_t}$ is the resistance of transmitting coil, and $\mathrm{R_{t-rad}}$ is the equivalent resistance of the transmitting coil radiation. Combining (4) and (5) then allows the efficiency to be expressed as

$$\eta = \frac{\mathrm{R_S}}{\mathrm{R_S} + \mathrm{R_t} + \mathrm{R_{t-rad}}} \cdot \frac{\mathrm{R_L}}{\mathrm{R_L} + \mathrm{R_r} + \mathrm{R_{r-rad}}} \quad (6)$$

where

$$\mathrm{R_S} = \frac{\omega^2\mathrm{M}^2}{\mathrm{R_L} + \mathrm{R_r} + \mathrm{R_{r-rad}}}. \quad (7)$$

The efficiency expression shown in (6) is therefore the product of the transmitter efficiency ($\frac{\mathrm{R_S}}{\mathrm{R_S}+\mathrm{R_t}+\mathrm{R_{t-rad}}}$) and the receiver efficiency ($\frac{\mathrm{R_L}}{\mathrm{R_L}+\mathrm{R_r}+\mathrm{R_{r-rad}}}$).

2) Multi-Transmitter Multi-Receiver (MTMR) System: The proposed system layout shown in Fig. 2 includes a transmitting subsystem with phase-shifted current drives, a receiving-coil subsystem comprising multiple receiving coils with electric loads, and a power electronics subsystem including the DC/AC inverter and power amplifiers. The transmitting subsystem is a balanced coil structure so that the amplitude of the resulting magnetic field can be approximately uniform with proper angle settings, similar to the rotating magnetic field of electric machines. Individual current sources with proper phase shifts drive the transmitting coils.

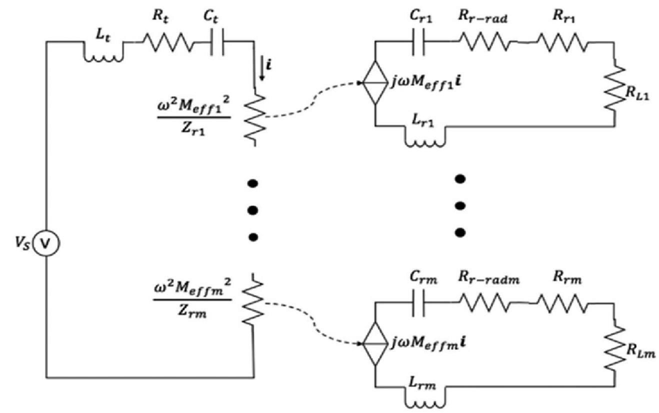

Fig. 2. Equivalent circuit for MTMR WPT system.

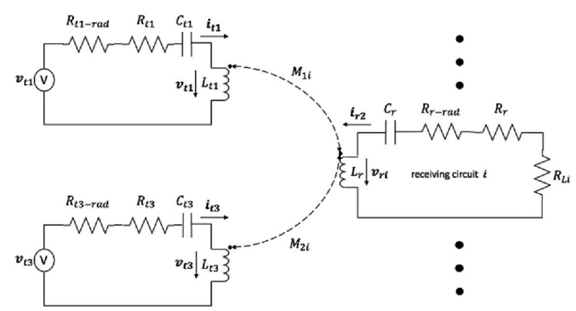

(a) Circuit model of a 2-coil system

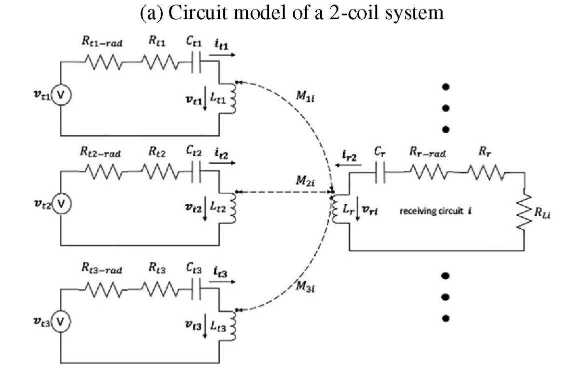

(b) Circuit model of a 3-coil system

Fig. 3. Multi-Transmitter Multi-Receiver (MTMR) Systems

Two balanced structures are proposed and found to achieve a uniform-amplitude magnetic field, and hence a nearly uniform efficiency at the resonant frequency. These two structures are 2-coil and 3-coil systems. A practical objective is to use the fewest possible coils to achieve uniform efficiency, thereby maintaining a competitive edge on cost. However, an additional coil may bring a cost saving in other aspect. For example, a 3-coil system can save 4 switches compared with a 2-coil system on the AC-DC-AC conversion. Circuit models of the 2-coil and 3-coil WPT systems are shown in Fig. 3(a) and 3(b), respectively. On the transmitting side, each coil has the same model, and the mutual inductances among them is zero owing to the orthogonal structure. Therefore, no mutual inductance exists on the transmitting side. Between the transmitting side and receiving side, mutual inductances are created by the interaction of the transmitting coils and multiple receiving coils, denoted as M_{1i}, M_{2i}, and M_{3i} (if 3-coil), respectively.

For a general MTMR with n transmitting coils and m receiving coils, similar to the STSR case, the relation between the coil voltage and currents can be described by

$$\begin{bmatrix} v_{t_1} \\ \vdots \\ v_{t_n} \\ v_{r_1} \\ \vdots \\ v_{r_m} \end{bmatrix} = j\omega \cdot \begin{bmatrix} L_{t1} & \cdots & M_{T1n} & M_{11} & \cdots & M_{1m} \\ \vdots & \ddots & \vdots & \vdots & \ddots & \vdots \\ M_{Tn1} & \cdots & L_{tn} & M_{n1} & \cdots & M_{nm} \\ M_{11} & \cdots & M_{1n} & L_{r1} & \cdots & M_{R1m} \\ \vdots & \ddots & \vdots & \vdots & \ddots & \vdots \\ M_{m1} & \cdots & M_{mn} & M_{Rm1} & \cdots & L_{rm} \end{bmatrix} \cdot \begin{bmatrix} i_{t_1} \\ \vdots \\ i_{t_n} \\ i_{r_1} \\ \vdots \\ i_{r_m} \end{bmatrix}, \tag{8}$$

where M_{Tij} represents the mutual inductance between the transmitting coils, M_{Rij} represents the mutual inductance between the receiving coils, L_{Ti} represents the self-inductance of the transmitting coils, and L_{Ri} represents the self-inductance of the receiving coils. In this case, because the transmitting coils are orthogonal, $M_{Tij} = 0$ Furthermore, the mutual inductances between receiving coils are ignored in comparison to the mutual inductances between transmitting and receiving coils. As taken from (8), the voltages of the receiving coils are

$$\begin{bmatrix} v_{r_1} \\ \vdots \\ v_{r_m} \end{bmatrix} = j\omega \cdot \begin{bmatrix} M_{11} & \cdots & M_{1n} & L_{r1} & \cdots & 0 \\ \vdots & \ddots & \vdots & \vdots & \ddots & \vdots \\ M_{m1} & \cdots & M_{mn} & 0 & \cdots & L_{rm} \end{bmatrix} \cdot \begin{bmatrix} i_{t_1} \\ \vdots \\ i_{t_n} \\ i_{r_1} \\ \vdots \\ i_{r_m} \end{bmatrix}. \tag{9}$$

Separately, the voltage of each receiving coil can be represented by

$$v_{r_i} = -\left(R_{ri} + R_{r-radi} + R_{Li} + \frac{1}{j\omega C_{ri}}\right) \cdot i_{r_i}, \tag{10}$$

where i is from 1 to m. The transmitting coil currents are defined as

$$i_{t_i} = i_t \cdot \beta_i \cdot e^{\alpha i}, \tag{11}$$

where i_t is the normal current of the transmitting coil-set, and β_i and α_i are the normalized amplitude coefficient and phase of corresponding transmitting coils.

When all transmitting and receiving coils resonate at the same frequency, similar to the STSR case, the ratio of the norm of the transmitter current to the receiver current is

$$\frac{i_t}{i_{ri}} = \frac{R_{ri} + R_{r-radi} + R_{Li}}{\omega M_{effi}} \tag{12}$$

The efficiency is again defined as (13) as shown at the bottom of the next page. Substituting (12), the efficiency becomes

$$\eta = \frac{R_S}{R_S + R_t} \cdot \sum_{i=1}^{n} \frac{R_{Si}}{R_S} \cdot \frac{R_{Li}}{R_{Li} + R_{ri} + R_{r-radi}}, \tag{14}$$

where

$$R_t = \sum_{i=1}^{n} {\beta_i}^2 \left(R_{ti} + R_{t-radi}\right) \ , \tag{15}$$

$$R_s = \sum_{i=1}^{m} R_{si} \ , \tag{16}$$

$$R_{si} = \frac{\omega^2 {M_{effi}}^2}{R_{Li} + R_{ri} + R_{r-radi}} \ , \tag{17}$$

$$M_{effi} = \sum_{j=1}^{n} M_{ji} \beta_j e^{\alpha j} \ . \tag{18}$$

M_{effi} is the effective mutual inductance of the corresponding receiving coil. Substituting (15)–(18), (14) becomes

$$\eta = \frac{\sum_i k_{1i} {M_{effi}}^2}{R_t + \sum_i k_{2i} {M_{effi}}^2} \ , \tag{19}$$

where

$$k_{2i} = \frac{\omega^2}{R_{Li} + R_{ri} + R_{r-radi}} \ , \tag{20}$$

$$k_{1i} = \frac{\omega^2 R_{Li}}{\left(R_{Li} + R_{ri} + R_{r-radi}\right)^2} \ . \tag{21}$$

The expression (19) shows a non-linear relationship between efficiency and effective mutual inductance. The efficiency also depends on a combination of resistances that are constant at a given frequency ω. Overall, the efficiency is impacted by the effective mutual inductance of multiple receivers at a given frequency. Finally, the ratio of an individual load power to the total input power to the transmitting coil is

$$P_i/P_t = \frac{R_{Si}}{R_S + R_t} \cdot \frac{R_{Li}}{R_{Li} + R_{ri} + R_{r-radi}} . \tag{22}$$

The expressions for efficiency and receiver power can be understood by the equivalent circuit of the MTMR WPT system shown in Fig. 2, where $Z_{Li} = R_{ri} + R_{r-radi} + R_{Li} + \frac{1}{j\omega C_{ri}} + j\omega L_{ri}$.

B. Effective Mutual Inductance

The mutual inductance between two coils [29] is

$$M = \frac{\mu_0}{4\pi} \oint_{L'} \oint_{L} \frac{Idl}{r} dl' , \tag{23}$$

where L and L' are curve following the two coils. The effective mutual inductance can be calculated by (18) thereafter.

As shown in Fig. 4, the 2-coil system comprises two vertical coils, and the 3-coil system comprises three tilted coils. The table-plane shows any two transmitting coils are orthogonal to each other in both structures. The normal vectors of the 2-coil system are (1, 0, 0) and (0, 1, 0); and of the 3-coil system are $(-\frac{1}{\sqrt{2}}, +\frac{1}{\sqrt{6}}, -\frac{1}{\sqrt{3}})$, $(+\frac{1}{\sqrt{2}}, +\frac{1}{\sqrt{6}}, -\frac{1}{\sqrt{3}})$ and $(0, -\frac{2}{\sqrt{6}}, -\frac{1}{\sqrt{3}})$. To measure the mutual inductance distribution, consider the table-plane with the receiving coil facing the z axis (coil A in Fig. 4) and the sphere with the receiving coil facing the radial direction (coil B in Fig. 4). Fig. 5 shows the flowchart of the phase-shift control method. The operating mode is automatically selected between 2-phase and 3-phase based on environmental parameters.

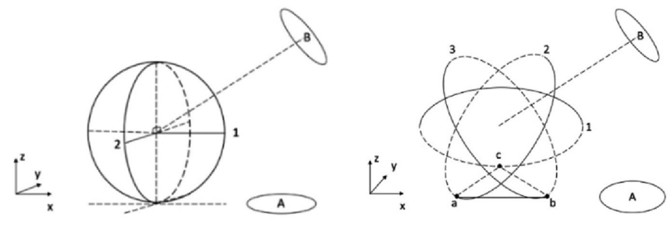

(a) (b)

Fig. 4. Placement of transmitting and receiving coils: (a) 2-Coil; (b) 3-Coil.

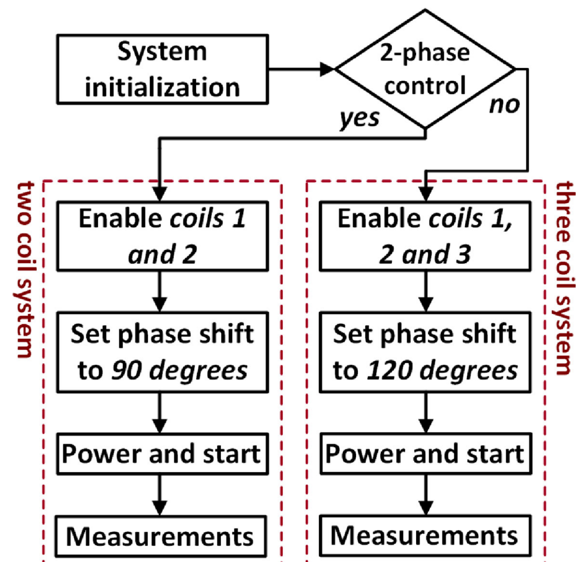

Fig. 5. Flowchart of phase-shift control.

For evaluation purposes, the radius of each transmitting coil is set to 7.5 cm, and each receiving coil to 5 cm. The effective planar mutual inductance with and without the phase-shift control for the 2-coil structure are shown in Fig. 6(a) and 6(b), respectively, and for the 3-coil structure in Fig. 7(a) and 7(b), respectively. These figures show that when the currents are not phase shifted, the effective mutual inductance is high only at two quadrants for the 2-coil structure. For the 3-coil structure, it is only high at the center where a receiver cannot be placed. Comparing Fig. 6(a) and 6(b), and Fig. 7(a) and (b) it is apparent that a proper phase-shift of the driven currents can generate a nearly equal and

$$\eta = \frac{\sum_{i=1}^{m} \mathbf{i}_{ri} \times {\mathbf{i}_{ri}}^* \cdot R_{Li}}{\sum_{i=1}^{n} \mathbf{i}_{ti} \times {\mathbf{i}_{ti}}^* \cdot \left(R_{ti} + R_{t-radi}\right) + \sum_{i=1}^{m} \mathbf{i}_{ri} \times {\mathbf{i}_{ri}}^* \cdot \left(R_{ri} + R_{r-radi} + R_{Li}\right)} \tag{13}$$

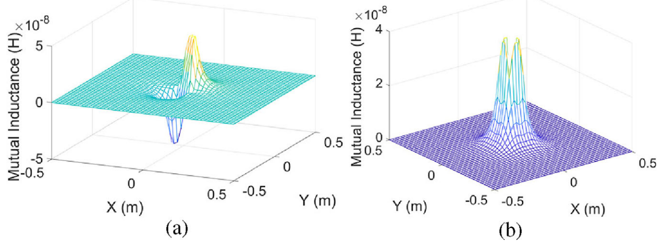

Fig. 6. Planar effective mutual inductance distribution of the 2-Coil structure: (a) without phase shift; (b) with 90 degrees phase shift.

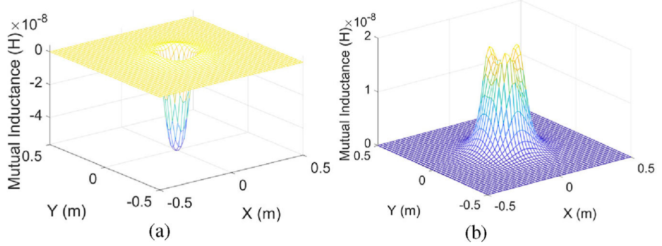

Fig. 7. Planar effective mutual inductance distribution of the 3-Coil Structure: (a) without phase shift; (b) with 120 degrees phase shift.

strong effective mutual inductance all around the transmitter if the receiving coil is placed on the table plane.

The directional diagram of a spherical mutual inductance distribution with 20 cm radius for the 2-coil and 3-coil structures are shown in Figs. 8 and 9, respectively. In a manner analogous to the radiation pattern of an antenna, under the spherical coordinates, the radii to the surfaces represent the absolute value of the mutual inductance of the receiving coil placed at a corresponding angle with a radial orientation. By comparing Fig. 8(a) to Fig. 8(b), and Fig. 9(a) to Fig. 9(b), it is apparent that the use of proper phase-shifts for drive currents can enhance the mutual inductance around the entire 3-D space in the vicinity.

C. Efficiency

1) Efficiency Distribution of Single Receiver: The number of turns for transmitting and receiving coils of the two structures are set to 20 and 10, respectively. In this case, the resistance density of the wire is 0.51 Ω/m at 2 MHz for Litz wire with a diameter of 1.5 mm. To find the optimum load resistance, the first derivative of the efficiency as a function of load resistance is used, as outlined in [2]. The appropriate load resistance is

$$\mathrm{R_L} = \sqrt{(\mathrm{R_r} + \mathrm{R_{r-rad}})^2 + \frac{(\mathrm{R_r} + \mathrm{R_{r-rad}})\,(\omega \mathrm{M})^2}{\mathrm{R_t} + \mathrm{R_{t-rad}}}}. \tag{24}$$

Correspondingly, the optimized efficiency distributions for a single receiver at 2 MHz for the two structures driven by phase-shifted currents are shown in Figs. 10 and 11.

2) Efficiency of Multiple Receivers and Minimum Receiving Power among Users: The efficiency of multiple receivers, denoted as Eff., and the minimum receiving power among users, denoted as $\mathrm{P_{ratio-min}}$, are two important factors that determine

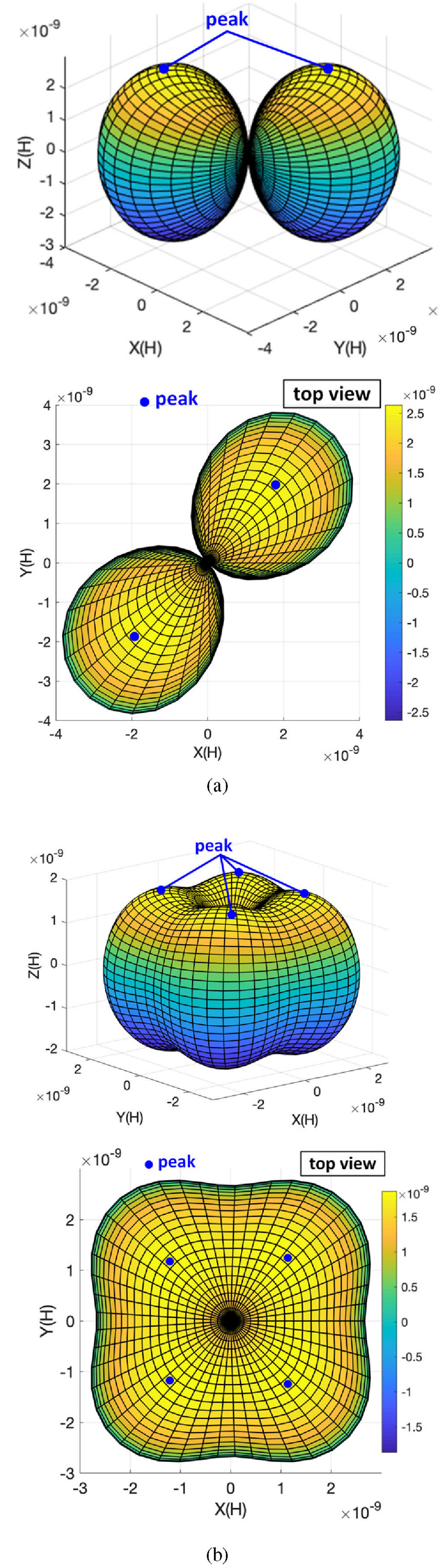

Fig. 8. 2-coil structure: directional diagram of effective mutual inductance distribution on the sphere: (a) effective mutual inductance without phase shift; (b) effective mutual inductance with 90 degrees phase shift.

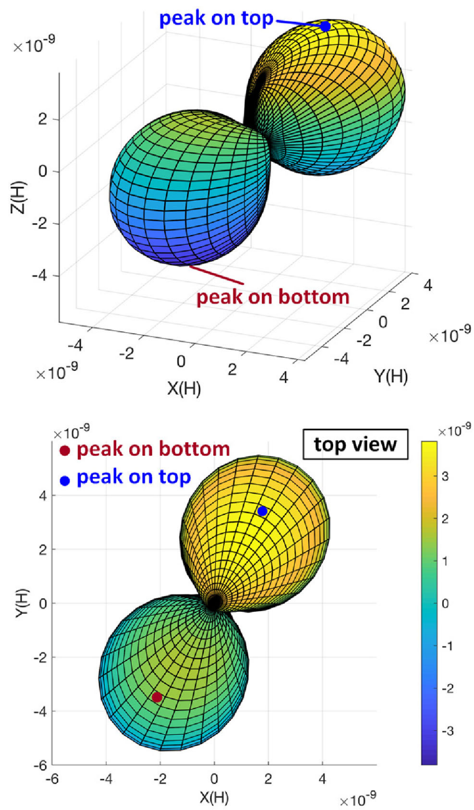

(a)

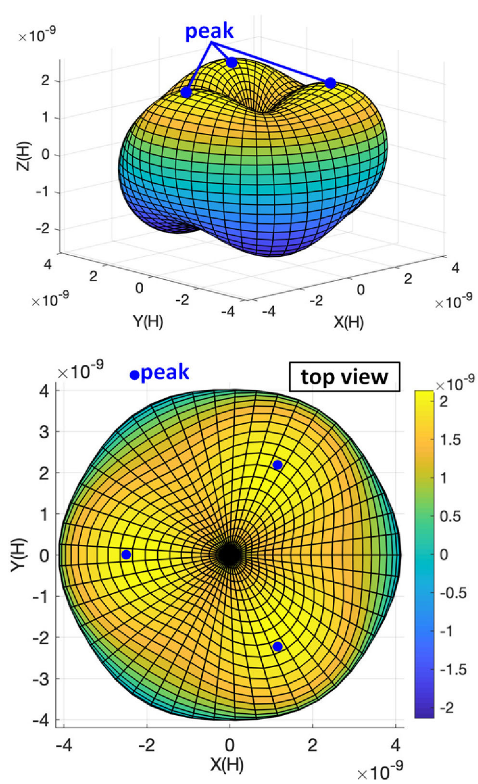

(b)

Fig. 9. 3-coil structure: directional diagram of effective mutual inductance distribution on the sphere. (a) effective mutual inductance without phase shift; (b) effective mutual inductance with 120 degrees phase shift.

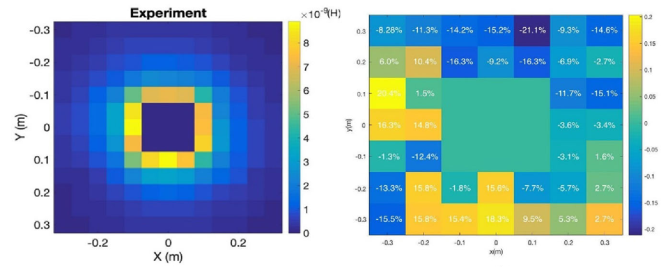

(a) (b)

Fig. 10. Experimental results of the effective mutual inductance for the 2-Coil structure: (a) measurement results; (b) error (experiment versus theory).

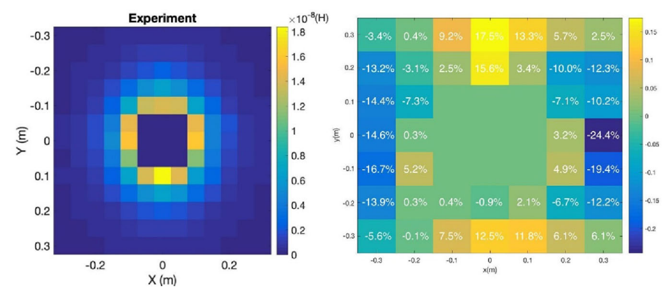

(a) (b)

Fig. 11. Experimental results of effective mutual inductance for the 3-coil structure: (a) measurement results; (b) error (experiment versus theory).

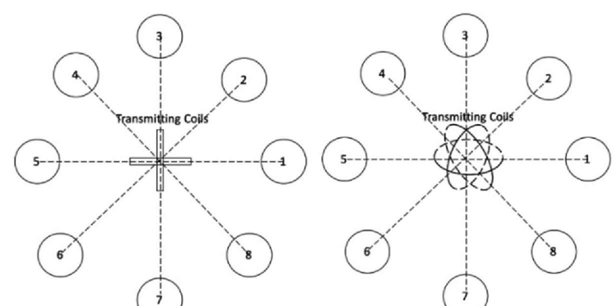

(a) (b)

Fig. 12. Top view of WPT structures with multiple receivers: (a) 2-Coil; (b) 3-Coil.

the charging quality of WPT. Referring to Fig. 12, three cases are analyzed:

(i) 4 receivers placed at 1, 3, 5 and 7; (ii) 4 receivers placed at 2, 4, 6, and 8; (iii) 8 receivers placed at all positions.

The operating frequency is set at 2 MHz as it is near the optimal operating point for the highest efficiency. The receivers are 15 cm away from the transmitter and all load resistances are 5 Ω. Table I show the minimum power ratio (lowest individual receiving power over input power) and overall power efficiency (total receiving power over input power) of the 2-coil structure and 3-coil structure. Note "C. V." stands for current vector, which is the vector of the normalized current coefficient β. As can be seen from the rightmost column in Table I, where appropriate phase-shifts are applied, the power transfer, hence the efficiency, is drastically increased with proper phase shifts,

TABLE I
THE 2-COIL(TOP) & 3-COIL(BOTTOM) STRUCTURE FOR MULTI-USER

C.V. / case	$\frac{1}{\sqrt{2}}[1,1]$ Eff.	$\frac{1}{\sqrt{2}}[1,1]$ $P_{ratio-min}$	$[1,0]$ Eff.	$[1,0]$ $P_{ratio-min}$	$\frac{1}{\sqrt{2}}[1,e^{\frac{j\pi}{2}}]$ Eff.	$\frac{1}{\sqrt{2}}[1,e^{\frac{j\pi}{2}}]$ $P_{ratio-min}$
i	57.66%	14.42%	57.66%	0.00%	57.66%	14.42%
ii	65.11%	0.00%	65.11%	8.98%	65.11%	8.98%
iii	68.15%	0.00%	68.15%	0.00%	68.15%	5.92%

C.V. / case	$\frac{1}{\sqrt{3}}[1,1,1]$ Eff.	$\frac{1}{\sqrt{3}}[1,1,1]$ $P_{ratio-min}$	$[1,0,0]$ Eff.	$[1,0,0]$ $P_{ratio-min}$	$\frac{1}{\sqrt{3}}[1,e^{\frac{j\pi}{3}},e^{\frac{j2\pi}{3}}]$ Eff.	$\frac{1}{\sqrt{3}}[1,e^{\frac{j\pi}{3}},e^{\frac{j2\pi}{3}}]$ $P_{ratio-min}$
i	55.65%	7.79%	67.02%	2.88%	68.58%	15.90%
ii	55.46%	10.11%	66.09%	0.15%	68.61%	15.85%
iii	64.22%	4.52%	71.02%	0.07%	72.15%	8.35%

TABLE II
BENCHMARK COMPARISON

WPT Methods	Multi-Charge	Dist. Charge	2-D Position-Free	3-D Position Free	Uniform Eff.
Proposed	Y	Y	Y	Y	Y
Witricity [1]	N	Y	N	N	N
MagMIMO [22]	N	Y	Y	Y	N
Qi Charging [2-7]	Y	N	N	N	N
2-Coil [35]	Y	Y	Y	N	N
3-Coil [36, 37]	Y	Y	Y	N	N
4-Coil [38, 39]	Y	Y	Y	N	N

availing simultaneous power delivery to all users. Fig. 12 shows the vertical view.

D. Benchmark Comparison

Current WPT technologies are overviewed in [21]. The representative methods [1]–[7], [22], [35]–[39] as mentioned in the Introduction section are Witricity and other multi-coil formations (resonant inductive charging), MagMIMO (position-free charging), and Qi (contacted). A detailed list below in Table II shows the advantages of the proposed system over other methods on multiple features.

III. SIMULATION AND EXPERIMENTAL RESULT

A. Experiment Setup

The proposed system consists of a transmitting subsystem configured as either 2-coil or 3-coil, a receiving subsystem, which includes multiple receiving coils with loads, and a power electronics system comprising a signal generator and power amplifiers. The experiment setup is shown in Fig. 13. Power Amp1 is Amplifier Research Model 150A100B with 150 W output, 10 kHz – 100 MHz, 55 dB gain (nominal), Power Amp 2 is ENI Model 3100LA RF Power Amplifier with 100 W output, 250 kHz – 1500 MHz, 55 dB (nominal). The oscilloscope is Tektronix 4-Channel 1 GHz. The signal generator is KKmoon MHS-5200A with the sampling rate at 200 Ms/s. The operating power range has been chosen to be within 0–10 W. Voltages and currents of input and output are measured to obtain power values. The operating voltage range and the current range for the transmitter coil are 0–10 V and 0–1 A, respectively, and those for the receiver coil are 0–5 V and 0–2 A, respectively.

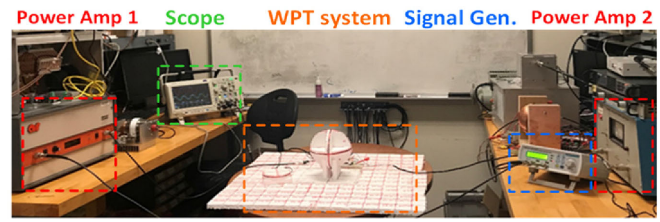

Fig. 13. Experiment test bench.

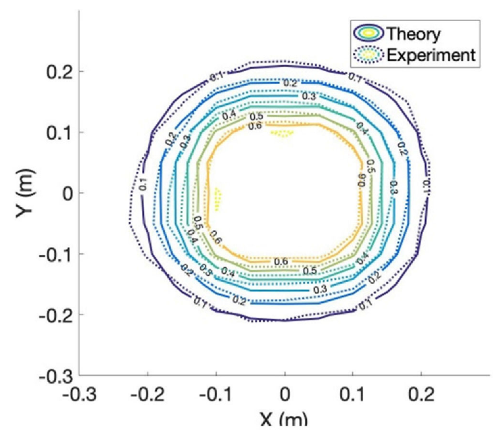

Fig. 14. Efficiency distribution of the 2-coil structure.

B. Case 1: 2-Coil Structure, 90 Degrees Phase Shift (2 MHz)

Based on (9), the open-circuit voltage of a single receiver is linear with the normal transmitting current at a fixed frequency. Therefore, the effective mutual inductance between one loop of a transmitting coil and one loop of a receiving coil can be measured by the ratio of open-circuit voltage of the receiving coil V_{r-open} to the normal current of the transmitting coil i_t.

$$M_{eff} = \frac{V_{r-open}}{i_t \cdot n_r \cdot n_t} \tag{25}$$

The measurement results of the effective mutual inductance are shown in Fig. 10(a). The error rate namely the difference between the experimental results and theoretical calculations based on the model of Section II, ranges from -21% to 16% with an average of 10.3% as shown in Fig. 10(b). This relatively low error rate demonstrates the close match between experiment and theory.

$$\delta = \frac{M_{exp} - M_{theory}}{M_{theory}} \tag{26}$$

The efficiency distribution of a single receiving coil with the optimized load resistance by (24) is measured by the ratio of receiving power to transmitting power, which is shown in Fig. 14.

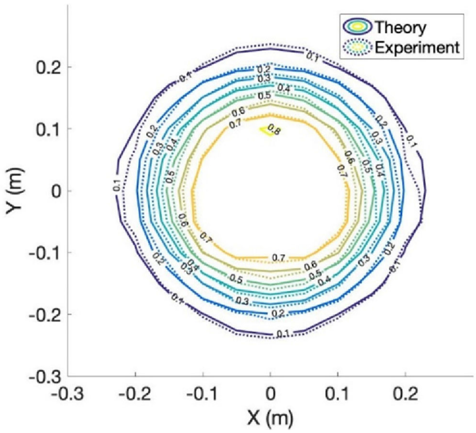

Fig. 15. Efficiency distribution of the 3-coil structure.

TABLE III
EXP. RESULT OF THE 2-COIL & 3-COIL STRUCTURE

Case	Measure	2-Coil Input Power	2-Coil Output Power	3-Coil Input Power	3-Coil Output Power
i	Theory	5.50	3.17	5.50	3.77
	Experiment	5.51	3.25	5.51	3.78
ii	Theory	5.50	3.75	5.50	3.89
	Experiment	5.52	3.79	5.52	3.88
iii	Theory	5.50	3.85	5.50	4.02
	Experiment	5.51	3.89	5.51	4.00

Case	Measure	2-Coil Efficiency	2-Coil $P_{ratio-min}$	3-Coil Efficiency	3-Coil $P_{ratio-min}$
i	Theory	57.66%	14.42%	68.61%	15.85%
	Experiment	58.97%	12.02%	68.54%	12.81%
ii	Theory	68.11%	17.03%	70.89%	15.89%
	Experiment	68.64%	13.79%	70.37%	15.19%
iii	Theory	70.08%	4.70%	72.89%	6.77%
	Experiment	70.52%	3.13%	72.69%	4.39%

C. Case 2: 3-Coil Structure, 120 Degress Phase Shift (2 MHz)

The effective mutual inductance for the 3-coil structure is shown in Fig. 11(a). The error rate ranges from –24.4% to 17.5% with an average of 8.03% as shown in Fig. 11(b). The efficiency distribution of a single receiving coil with the optimized load resistance by (24) is shown in Fig. 15. The overall efficiency and the minimum receiving power are shown in Table III.

Case 2 with phase-shifts of 120 degrees shows an even higher efficiency in the 3-D space, ensuring the broader and more uniform high-efficiency charging range. It may lead to extra material in comparison to Case 1 with a phase-shift of 90 degrees. Depending on the coil material, the extra cost may be significant.

The overall efficiency and the minimum receiving power with 4 and 8 receivers with load resistance of 5 Ω placed in the positions shown in Fig. 14 with the distance of 15 cm to the center is shown in Table III in regards to C2 in Section II, where the minimum receiving power ratio is defined as the receiving power over the total input power. Further calculations yield the average efficiency of 66.04% and the variance of 0.26 for the 2-coil system and the average efficiency of 70.53% and the variance of 0.03 for the 3-coil system. These indicate the 3-coil system brings an improvement of 6.8% on the average efficiency and a reduction of 88.7% on the variance.

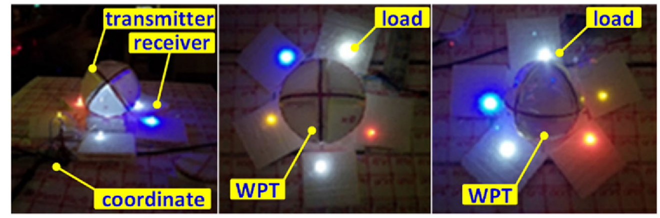

(a) (b) (c)

Fig. 16. Demonstrations: (a) WPT set-up; (b) 2-coil structure; (c) 3-coil structure.

D. Demonstration

For the purposes of illustration, colorful LEDs are used to emulate the electric load as shown in Fig. 16(a). The opreations of the 2-coil structure and the 3-coil structure are shown in Fig. 16(b) and 16(c), respectively.

IV. CONCLUSION

For WPT systems, an effective method to create a quasi-uniform efficiency in a 3-D space around the transmitting system is proposed and examined theoretically and experimentally. The key novelty is the application of a phase-shifting method on balanced magnetic coil structures – a clear distinction from a traditional non-phase shifting method. The 3-coil structure is verified to have a more robust efficiency delivery with 88.7% reduction on the variance, compared with the 2-coil structure. Experimental results have verified the theoretical calculations with less than 10% average error rate. The study shows that:

1) The effective mutual inductance distribution around the transmitter is quasi-uniform when the transmitting coil-set is driven by properly phase-shifted currents;
2) The rotating magnetic field generated by phase-shifted currents will form a quasi-uniform efficiency distribution for single user, and higher minimum receiving power ratio for multiple users; and
3) The 3-coil structure driven by 120 degrees phase-shift current shows a better performance – a higher and more stable efficiency, compared with the 2-coil structure driven by a 90 degrees phase-shift current, a lower variance (reduced by 88.7%), and an improved average efficiency (by 6.8%).

To summarize, the proposed WPT system shows robustness and flexibility to the receivers' position and orientation in a complicated multi-user environment. The overall efficiency can be improved as future work by customizing dynamic phase-shift based on users' position or advanced coils with lower resistance.

REFERENCES

[1] A. Kurs, A. Karalis, R. Moffatt, J. D. Joannopoulos, P. Fisher, and M. Soljacic, "Wireless power transfer via strongly coupled magnetic resonances," *Science*, vol. 317, no. 5834, pp. 83–86, Jul. 2007.

[2] S. L. Ho, J. Wang, W. N. Fu, and M. Sun, "A comparative study between novel witricity and traditional inductive magnetic coupling in wireless charging," *IEEE Trans. Magnetics*, vol. 47, no. 5, pp. 1522–1525, Apr. 2011.

[3] J. D. Jackson, *Classical Electrodynamics*. Hoboken, NJ, USA: Wiley, 2007, pp. 413–416.

[4] J. Kim, G. Wei, M. Kim, J. Jong, and C. Zhu, "A comprehensive study on composite resonant circuit-based wireless power transfer systems," *IEEE Trans. Ind. Electron.*, vol. 65, no. 6, pp. 4670–4680, Nov. 2017.

[5] Carobolante, P. Menegoli, F. Marino, and N. Jeong, "A novel charger architecture for resonant wireless power transfer," *IEEE J. Emerg. Sel. Topics Power Electron.*, vol. 6, no. 2, pp. 571–580, Feb. 2018.

[6] M. R. Basar, M. Y. Ahmad, J. Cho, and F. B. Ibrahim, "An improved wearable resonant wireless power transfer system for biomedical capsule endoscope," *IEEE Trans. Ind. Electron.*, vol. 65, no. 10, pp. 7772–7781, Feb. 2018.

[7] K. Song *et al.*, "EMI reduction methods in wireless power transfer system for drone electrical charger using tightly-coupled three-phase resonant magnetic field," *IEEE Trans. Ind. Electron.*, vol. 65, no. 9, pp. 6839–6849, Jan. 2018.

[8] C. Cai *et al.*, "Resonant wireless charging system design for 110 kV high voltage transmission line monitoring equipment," *IEEE Trans. Ind. Electron.*, vol. 66, no. 5, pp. 4118–4129, Feb. 2018.

[9] A. Abdolkhani, A. P. Hu, and C. Nair, "A double stator through-hole type contactless slipring for rotary wireless power transfer applications," *IEEE Trans. Energy Convers.*, vol. 29, no. 2, pp. 426–434, Jun. 2014.

[10] M. Liu, K. W. Chan, J. Hu, Q. Lin, J. Liu, and W. Xu, "Design and realization of a coreless and magnetless electric motor using magnetic resonant coupling technology," *IEEE Trans. Energy Convers.*, vol. 34, no. 3, pp. 1200–1212, Sep. 2019.

[11] H. Zeng and F. Z. Peng, "SiC-based Z-source resonant converter with constant frequency and load regulation for EV wireless charger," *IEEE Trans. Power Electron.*, vol. 32, no. 11, pp. 8813–8822, Dec. 2016.

[12] B. H. Choi, V. X. Thai, E. S. LEE, J. H. Kim, and C. T. Rim, "Dipole-coil-based wide-range inductive power transfer systems for wireless sensors," *IEEE Trans. Ind. Electron.*, vol. 63, no. 5, pp. 3158–3167, Jan. 2016.

[13] L. Shi *et al.*, Wireless power hotspot that charges all of your devices. *MobiCom*, Sep. 2015.

[14] H. Yin, M. Fu, M. Liu, J. Song, and C. Ma, "Autonomous power control in a reconfigurable 6.78 megahertz multiple-receiver wireless charging system," *IEEE Trans. Ind. Electron.*, vol. 65, no. 8, pp. 6177–6187, Dec. 2017.

[15] A Berger, M. Agostinelli, S. Vesti, J. A. Oliver, J. A. Cobos, and M. Huemer, "A wireless charging system applying phase-shift and amplitude control to maximize efficiency and extractable power," *IEEE Trans. Power Electron.*, vol. 30, no. 11, pp. 6338–6348, Nov. 2015.

[16] Y. Cao, Z. Dang, J. A. Dahouq, and E. Phillips, "Dynamic efficiency tracking controller for reconfigurable four-coil wireless power transfer system," in *Proc. IEEE Appl. Power Electron. Conf. Expo.*, pp. 3684–3689, May 2016.

[17] X. Lu, P. Wang, D. Niyato, D. Kim, and Z. Han, "Wireless charger networking for mobile devices: Fundamentals, standards, and network applications," *IEEE Commun. Surveys Tutorials*, vol. 22, no. 2, pp. 126–135, Apr. 2015.

[18] X. Lu, P. Wang, D. Niyato, D. Kim, and Z. Han, "Wireless charging technologies: Fundamentals, standards, and network applications," *IEEE Commun. Surv. Tutorials*, vol. 18, no. 2, pp. 1413–1452, Nov. 2015.

[19] Z. N. Low, R. A. Chinga, R. Tseng, and J. Lin, "Design and test of a high-power high-efficiency loosely coupled planar wireless power transfer system," *IEEE Trans. Ind. Electron.*, vol. 56, no. 5, pp. 1801–1812, May 2009.

[20] T. C. Beh, M. Kato, T. Imura, S. Oh, and Y. Hori, "Automated impedance matching system for robust wireless power transfer via magnetic resonance coupling," *IEEE Trans. Ind. Electron.*, vol. 60, no. 9, pp. 3689–3698, Jul. 2012.

[21] L. Xie, Y. Shi, Y. T. Hou, and W. Lou, "Wireless power transfer and applications to sensor networks," *IEEE Wireless Commun.*, vol. 20, no. 4, pp. 140–145, Aug. 2013.

[22] J. Jadidian and D. Katabi, "Magnetic MIMO: How to charge your phone in your pocket," in *Proc. 20th Annu. Int. Conf. Mobile Comput. Netw., ACM*, 2014.

[23] G. Yang, M. R. V. Moghadam, and R. Zhang, "Magnetic MIMO signal processing and optimization for wireless power transfer," *IEEE Trans. Signal Proc.*, vol. 65, no. 11, pp. 2860–2874, Feb. 2017.

[24] W. Ng, C. Zhang, D. Lin, and S. Y. Hui, "Two-and three-dimensional omnidirectional wireless power transfer," *IEEE Trans. Power Electron.*, vol. 29, no. 9, pp. 4470–4474, Sep. 2014.

[25] P. Sun, Y. Dong, and H. YE, H. Zhao "A wireless power transfer CPS based on 2D omni-directional rotating magnetic field," in *Proc. Software Quality, Rel. Security Companion, IEEE Int. Conf.*, 2016, pp. 252–258.

[26] D. Lin, C. Zhang, and S. Y. Hui, "Mathematic analysis of omnidirectional wireless power transfer—Part-I 2-dimensional systems," *IEEE Trans. Power Electron.*, vol. 32, no. 1, pp. 625–633, Jan. 2017.

[27] D. Lin, C. Zhang, and S. Y. Hui, "Mathematic analysis of omnidirectional wireless power transfer—Part-II three-dimensional systems," *IEEE Trans. Power Electron.*, 2017, vol. 32, no. 1, pp. 613–624, Jan. 2017.

[28] J. Zhao, X. Huang, and W. Wang, "Wireless power transfer with two-dimensional resonators," *IEEE Trans. Magn.*, vol. 50, no. 1, pp. 1–4, Jan. 2014.

[29] J. A. Wheeler and R. P. Feynman, "Classical electrodynamics in terms of direct interparticle action," *J. Rev. Modern Phys.*, vol. 21, no. 3, pp. 180–181, 1949.

[30] P. C. Krause, O. Wasynczuk, T. C. O'Connell, and M. Hasan, "Tesla's contribution to electric machine analysis," *IEEE Trans. Energy Convers.*, vol. 32, no. 2, pp. 591–598, Jun. 2017.

[31] S. D. Sudhoff and R. Sahu, "Metamodeling of rotating electric machinery," *IEEE Trans. Energy Convers.*, vol. 33, no. 3, pp. 1058–1071, Sep. 2018.

[32] O. Laldin, S. D. Sudhoff, and S. Pekarek, "An analytical design model for wound rotor synchronous machines," *IEEE Trans. Energy Convers.*, vol. 30, no. 4, pp. 1299–1309, Dec. 2015.

[33] J. A. Krizan and S. D. Sudhoff, "A design model for salient permanent-magnet machines with investigation of saliency and wide-speed-range performance," *IEEE Trans. Energy Convers.*, vol. 28, no. 1, pp. 95–105, Mar. 2013.

[34] Y. Zhang, T. Lu *et al.*, "Quasi-uniform magnetic field generated by multiple transmitters of magnetically-coupled resonant wireless power transfer," *IEEE ICEMS*, 2015, Oct. 2015.

[35] Y. Wang, J. Song, L. Lin, X. Wu, and W. Zhang, "Research on magnetic coupling resonance wireless power transfer system with variable coil structure," in *Proc. IEEE PELS Workshop Emerg. Technol.: Wireless Power Transfer*, Chongqing, 2017, pp. 1–6.

[36] F. Hattori, J. Imaoka, M. Yamamoto, and M. Masuda, "Fundamental experiment of 3-phase electric resonant coupling wireless power transfer," in *Proc. 7th Int. Conf. Renew. Energy Res. Appl.*, Paris, pp. 1417–1422, 2018.

[37] M. R. Basar, M. Y. Ahmad, J. Cho, and F. Ibrahim, "A 3-coil wireless power transfer system with fine tuned power amplifier for biomedical capsule," in *Proc. IEEE Asia Pacific Microw. Conf.*, Kuala Lumpar, pp. 142–145, 2017.

[38] S. Y. Tan, H. J. Lee, K. Y. Lau, and P. J. Ker, "Simulation of 4-coils magnetic resonance coupling for multiple receivers wireless power transfer at various transmission distance," in *Proc. IEEE Student Conf. Res. Develop.*, Selangor, Malaysia, pp. 1–5, 2018.

[39] C. Xu, Y. Zhuang, H. Han, C. Song, Y. Huang, and J. Zhou, "Multi-coil high efficiency wireless power transfer system against misalignment," in *Proc. IEEE MTT-S Int. Wireless Symp.*, Chengdu, pp. 1–3, 2018.

Nelson Xuntuo Wang (Student Member, IEEE) received the B.S. degree (with highest Hons.) in electrical engineering from General Motors Institute, the University of Michigan, MI, USA, in 2012, and the S.M. degree in electrical engineering and computer science from the Massachusetts Institute of Technology (MIT), Cambridge, MA, USA, in 2014, where he is currently working toward the Ph.D. degree in electrical engineering and computer science. He was a Cross-Registrant on the M.B.A. program with Harvard Business School, Boston, MA, USA. His current research interests include the analysis, design and control of power system, electric motor, and power electronics, and machine learning methods for energy data mining.

Dr. Wang was the recipient of the Irwin Jacobs Presidential Fellowship from MIT. Dr. Wang was named as a Forbes 30 Under 30 on Forbes magazine. He has been nominated as a 35 Under 35 on MIT Technology Review.

Han-Wei Wang (Student Member, IEEE) received the B. S. degree from Tsinghua University, Beijing, China, in 2019. He is currently working toward the Ph.D. degree with the Electrical and Computer Engineering Department of University of Illinois Urbana Champaign (UIUC). His research interests include metamaterial, nanophotonics and wireless power transfer (WPT). He was the recipient of the numerous awards in creative system design from Tsinghua University.

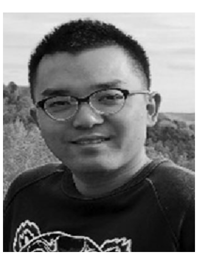

Jie Mei (Student Member, IEEE) received the B.S. degree in electrical engineering from the School of Electrical and Computer Engineering, Georgia Institute of Technology, Atlanta, GA, USA, in 2015. He is currently working toward the Ph.D. degree with the Department of Electrical Engineering and Computer Science, Massachusetts Institute of Technology, Cambridge, MA, USA. His research interests include electric machines, Multi-Carrier energy system, and electric vehicle technologies.

Sajjad Mohammadi (Student Member, IEEE) received the B.S. degree (Hons.) from the Kermanshah University of Technology, Kermanshah, Iran, in 2011 and the M.S. degree (Hons.) from the Amirkabir University of Technology, Tehran, in 2014, all in electrical engineering. He also received the M.S. degree in electrical engineering and computer science from the Massachusetts Institute of Technology (MIT), Cambridge, MA, where he is currently working toward the Ph.D. degree. His research interests include energy conversion, design and control of electromechanical devices and electric machines, drives, power electronics, power systems, and energy policy.

He attained a number of awards such as Best M.Sc. Thesis Awards from IEEE Iran Section and Amirkabir University of Technology, 2nd place in National Chem-E-Car Competitions 2009 held by Sharif University of Technology, 2nd place in the Humanoid Robots plus 1st place in Technical Challenge both in International Iran-Open 2010 Robotics Competitions in Tehran, and 1st place in the Humanoid Robots plus 1st place in Technical Challenge both in International AUTCUP 2010 Khwarizmi Robotics Competitions held by Amirkabir University.

Jinyeong Moon (Senior Member, IEEE) received the B.S. degree in electrical engineering and computer science from the Korea Advanced Institute of Science and Technology, Daejeon, South Korea, in 2005, the M.S. degree in electrical engineering from Stanford University, Stanford, CA, USA, in 2007, and the Ph.D. degree in electrical engineering and computer science from the Massachusetts Institute of Technology (MIT), Cambridge, MA, USA, in 2016. He is currently an Assistant Professor with electrical and computer engineering, Florida State University. He was with Hynix Semiconductor Inc., MIT, and Maxim Integrated as a Key Technical Member. He is currently an Associate Editor for Journal of Power Electronics and the Publication Liaison for IEEE Power Electronics Society's Technical Committee. His research interests include modeling, design, analysis, and measurement of circuits and systems in the fields of power conversion, energy harvesting, electromagnetics, and renewable energy.

Dr. Moon was the recipient of two grand prizes in the MIT Clean Energy Prize in 2014, and was a recipient of the Kwanjeong Scholarship and the Hynix Strategic Patent Award. He holds 17 registered U.S. and international patents.

Jeffrey H. Lang (Fellow, IEEE) received the S.B., S.M., and Ph.D. degrees from the Department of Electrical Engineering and Computer Science, Massachusetts Institute of Technology (MIT), Cambridge, MA, USA, in 1975, 1977, and 1980, respectively. He was the Associate Director with the MIT Laboratory for Electromagnetic and Electronic Systems between 1991 and 2003. He joined the Faculty of MIT in 1980, where he is currently the Vitesse Professor of electrical engineering. His research and teaching interests include the analysis, design, and control of electromagnetic and electromechanical systems with an emphasis on rotating machinery; micro/nanoscale (MEMS/NEMS) sensors, actuators and energy converters; flexible structures; and the dual use of electromechanical actuators as motion and force sensors. He has authored or coauthored more than 260 papers and holds 12 patents in the areas of electromechanics, MEMS, and power electronics and applied control. He was an Associate Editor of Sensors and Actuators between 1991 and 1994. He was also as the General Cochair and the Technical Cochair of the 1992 and 1993 IEEE MEMS Workshops, respectively, and the General Cochair of the 2013 PowerMEMS Conference. He is a Coauthor of Foundations of Analog and Digital Electronic Circuits (San Mateo, CA, USA: Morgan Kaufman, 2005), and the Editor of, and a contributor to, Multi-Wafer Rotating MEMS Machines: Turbines Generators and Engines (New York, NY, USA: Springer, 2009). Prof. Lang is a former Hertz Foundation Fellow. He was the recipient of the four Best Paper Prizes from IEEE societies, and has received two teaching awards from MIT.

James L. Kirtley, Jr. (Life Fellow, IEEE) received the Ph.D. degree from the Massachusetts Institute of Technology (MIT), Cambridge, MA, USA, in 1971. He is currently a Professor of Electrical Engineering with MIT. He has been with the Large Steam Turbine Generator Department, General Electric, Schenectady, NY, USA, as an Electrical Engineer, with Satcon, Boston, MA, USA, Technology Corporation as the Vice President and General Manager of the Tech Center and as the Chief Scientist, and with the Swiss Federal Institute of Technology, Zürich, Switzerland, as a Gastdozent. He continues as a Director of Satcon. He is a Specialist in electric machinery and electric power systems. He received the IEEE Third Millenium Medal in 2000 and the Nikola Tesla Prize in 2002.

Dr. Kirtley served as the Editor-in-Chief of the IEEE TRANSACTIONS ON ENERGY CONVERSION from 1998 to 2006 and continues to serve as an Editor for that journal and as a member of the Editorial Board of the *Electric Power Components and Systems* journal. He was elected to the United States National Academy of Engineering in 2007. He is a Registered Professional Engineer in Massachusetts.